

Authentication of stony meteorites by Raman spectroscopy and multivariate analysis

Alejandro González-Sánchez^{1,*}, Cuauhtémoc Araujo-Andrade^{1,a}, Claudio Frausto-Reyes^{2,b}, Edgar Esparza-Ibarra^{3,c} and Alejandro Gutiérrez-Rodríguez⁴

¹ Ciencia y Tecnología de la Luz y la Materia, Universidad Autónoma de Zacatecas, QUANTUM, Circuito Marie Curie s/n, 98160. Zacatecas, Mexico.

² Centro de Investigaciones en Óptica, A.C. Constitución 524, 20200, Gómez Morín, Aguascalientes, Mexico.

³ Unidad Académica de Biología Experimental. Universidad Autónoma de Zacatecas, Mexico.

⁴ Unidad Académica de Física. Universidad Autónoma de Zacatecas, Mexico.

*Corresponding author (A. González-Sánchez): alejandro.gonzalez@uaz.edu.mx

^a 0000-0001-7397-5093; ^b 0000-0002-5728-6455; ^c 0000-0002-6037-3998

EDITORS:

Peter Schaaf
Luigi A. Solari

HOW TO CITE:

González-Sánchez, A., Araujo-Andrade, C., Frausto-Reyes, C., Esparza-Ibarra, E. & Gutiérrez-Rodríguez, A. (2026). Authentication of stony meteorites by Raman spectroscopy and multivariate analysis. *Revista Mexicana de Ciencias Geológicas*, 43(1), 1–10. DOI: <https://dx.doi.org/10.22201/igc.20072902e.2026.1.1860>

Manuscript received: January 29, 2025

Corrected manuscript received: April 4, 2025

Manuscript accepted: April 6, 2025

Published Online: April 1, 2026

COPYRIGHT

© 2026 The Author(s).

This is an open-access article published and distributed by the Universidad Nacional Autónoma de México under the terms of a [Creative Commons Attribution 4.0 International License \(CC BY\)](https://creativecommons.org/licenses/by/4.0/) which permits unrestricted use, distribution, and reproduction in any medium, provided the original author and source are credited.



ABSTRACT

We propose a novel, fast, reliable and non-destructive method based on Raman spectroscopy and chemometrics for the analysis and authentication of rocky meteorites. We use the spectral information obtained from rocky samples to discriminate between ordinary terrestrial rocks (with morphology and observable characteristics like meteorites) and authentic meteorites. Applying unsupervised statistical methods, such as Principal Component Analysis, we can discriminate between both samples. Main discriminator being the bands ascribed to hematite, which is present in all the terrestrial samples. A classification model for the authentication of meteorites is calibrated using supervised methods, such as partial least square regression under the discriminant analysis modality (PLS-DA). The calibrated model was able to correctly classify meteorites and ordinary rocks with sensitivity and specificity values of 93 % and 90 %, respectively.

Keywords: Raman spectroscopy; multivariate analysis; meteorites authentication.

RESUMEN

Proponemos un método novedoso, rápido, confiable y no destructivo basado en espectroscopía Raman y quimiometría para el análisis y autenticación de meteoritos rocosos. Utilizamos la información espectral obtenida de muestras rocosas para discriminar entre rocas terrestres ordinarias (con morfología y características observables como meteoritos) y meteoritos auténticos. Aplicando métodos estadísticos no supervisados, como el Análisis de Componentes Principales, podemos discriminar entre ambas muestras, siendo el principal discriminador las bandas adscritas a hematita, presentes en todas las muestras terrestres. Se calibra un modelo de clasificación para la autenticación de meteoritos utilizando métodos supervisados, como la regresión de mínimos cuadrados parciales bajo la modalidad de análisis discriminante (PLS-DA). El modelo calibrado pudo clasificar correctamente meteoritos y rocas ordinarias con valores de sensibilidad y especificidad del 93 % y 90 %, respectivamente. La novedosa metodología propuesta es, por tanto, una forma factible y fiable de autenticar meteoritos.

Palabras clave: espectroscopía Raman; análisis multivariado; autenticación de meteoritos.

INTRODUCTION

Our insights of how planets and other major bodies in the Solar System formed are basically based on our understanding of the star formation process, protoplanetary disks and the study of meteorites. Early evidence of protoplanetary disks was obtained from submillimeter and infrared observations (Strom *et al.*, 1989; Wolf *et al.*, 2002; Cieza 2015; de Leon *et al.*, 2015; Benisty *et al.*, 2022, and Andrews 2020 for a review), asymmetric scattering of visual and near-infrared light (Zinnecker *et al.*, 1999; Takami *et al.*, 2023; Sturm *et al.*, 2023), line profiles (Edwards *et al.*, 1987; Bast *et al.*, 2011; Dong *et al.*, 2023), and the detection of stellar jets (Rodríguez & Reipurth 1994; Reipurth *et al.*, 1999, 2000; Ray & Ferreira 2021). Actually, the joint of capabilities of the James Webb Space Telescope (JWST) combined with the ALMA (Atacama Large Millimeter Array) survey of protoplanetary disks, and the Hubble Space Telescope (HST) combined with adaptive optics at large telescopes and millimeter interferometry from the ground, have enhanced the evidence for the presence of flattened structures around young stars such as in T Tauri (Ismailov *et al.*, 2022) and Haro-Herbig type (Bally & Devine 1994; Jensen & Akeson 2014). Moreover, some surveys (*e.g.*, Williams & Cieza 2014) imply that more than half of the youngest low mass pre-main sequence stars are associated with disks. Three key components in the formation of a star have been pointed out (Matzner & McKee 2000 and Montmerle *et al.*, 2006): an outer envelope, an inner accretion disk, and matter ejected perpendicular to the disk. The interplay between these components tends to form an inhomogeneous and turbulent disk of gas and dust. Local turbulence within the disk fragmentation into numerous gaseous protoplanets, and most of the solid particles get clustered up to form denser planetesimals. Whereas such a general vision of the formation of planetary disks is well accepted, the details of how our proto solar system evolved are encoded into the rich and wide gamut of substructures such as meteorites, asteroids and comets. Therefore, besides the authentication of these rocks, and obtaining information from them is fundamental to study these aspects.

From the last two decades, a number of projects and strategies have been used to quantify the amount of meteoritical material falling through Earth, which comprises satellite observations, meteor radar observations (Fries & Fries 2010; Hankey *et al.*, 2017), drones and machine learning, (Anderson *et al.*, 2020; Citron *et al.*, 2021; Anderson *et al.*, 2022) and laser observations of the sodium and iron atoms from evaporating objects in the atmosphere (*e.g.*, Pilkington & Grieve 1992; Campbell-Brown & Hildebrandt 2004; Oberst *et al.*, 2004; Milley *et al.*, 2007; Dudorov & Eretnova 2020). The accumulation of Ir and Os in the polar ice cores, especially in deep-sea sediments, helps to figure out a rough estimation of approximately 40–100 tons of meteorites fall on Earth every day. From them about 0.0001 % cover a range of masses between 10 g up to roughly 1 kg. Due to the random character of these deposits, the greatest extensions of sea, the daylight and the low density of population in vast surface regions of the planet, it is estimated that less than 8 % is observed. Bland *et al.* (1996) have performed an outstanding estimation of the meteoritic material fall during the last 50 millenniums. The ongoing projects such as SAMBA (Search for Antarctic Meteorites, 2010), FRIPON (Fireball Recovery and InterPlanetary Observation Network; Colas, 2020) which started in 2016, ARES (Astro Material Research and Exploration Science, 2023) and DOME (Detection and Observation of Meteorites, 2022) are providing valuable information even more exact and detailed of the size and type a number of particles that impact our planet and the atmosphere. Therefore, a reliable, non-destructive technique of authentication of meteorites is highly requested.

Briefly, the techniques available for the authentication of meteorites can be organized in two main groups; invasive (and some also destructive) and non-invasive ones. For example, SEM/EDS and electron probe analysis, are invasive surface measurement techniques. However, even when the SEM/EDS techniques can be used as a non destructive technique by adopting the variable pressure method, the mineralogical analysis is unable to identify polymorphs nor organic compounds potentially present in meteorites. A major breakthrough has been achieved in the authentication of pure metallic meteorites and mixed meteorites such as pallasites and mesosiderites, since once the material is polished and treated with nital to discover a peculiar geometrical pattern known as Widmanstätten which is not present in any terrestrial material (Goldstein & Ogilvie 1965; Yang & Goldstein 2005). For a non-invasive method, Raman spectroscopy allows characterization of materials trapped within transparent mineral grains such as olivine and pyroxene. Data collected from inclusions in chondrules mineral grains is a new Endeavor by Raman imagery that is providing new information relevant to the formation history and chemical environment during the formation of the oldest materials known in our solar system.

In the last few years, Raman spectroscopy has been used to study extraterrestrial material such as meteorites (Hochleitner *et al.*, 2004; Dobričá *et al.*, 2011; Nascimento-Dias *et al.*, 2021; Wang *et al.*, 2023; Donato *et al.*, 2023), Mars meteorites (Wang *et al.*, 2004; Steele *et al.*, 2007; Hutchinson *et al.*, 2014; Huidobro *et al.*, 2021; Malarewicz *et al.*, 2023), interplanetary dust (Stephan *et al.*, 1994), lunar rocks (Donaldson *et al.*, 2009; Greenhagen *et al.*, 2010) and cometary dust (*e.g.*, Ishiguro 2008). The characterization of carbonaceous matter in meteorites using Raman spectroscopy, is not new. This has been done in a sample of Antarctic meteorites by Dobričá *et al.* (2011) who reported that more than half of their sample contains a substantial amount of polyaromatic carbonaceous matter with a high degree of disorder. Raman spectroscopy demands only minimal sample preparation and has the advantage that the sample can be any solid, liquid or gas as long as it be optically accessible, with different indexes of opacity or with different surface textures. Therefore, even more recently it has been recognized that Raman spectroscopy and particularly micro-Raman spectroscopy as feasible methods for *in situ* planetary analysis (Musa *et al.*, 2021). Both of them will allow addressing crucial biological, organic and mineralogical analysis, such as: a) Chemical analysis of the mineral composition of planetary surfaces, b) identification of inorganic, organic or biological compounds, this being the main benefit that Raman spectroscopy offers, c) identification of rials in soils and rocks), d) classification of rocks (igneous, sedimentary and metamorphic) and definition of petrogenetic processes, e) oxidation state of planetary elements, f) content of volatiles and gaseous inclusions (H₂O, SO₃, CO₂, NO₂, H₂, O₂) in minerals and glasses, g) determination of selected minor and trace element contents (*e.g.* rare earth elements), h) determination of reaction kinetics, *i.e.* oxidation processes on newly exposed surfaces and determination of the reaction products, i) morphology of organic inclusions (fossils) and minerals on a micrometric scale, j) water and ice on *e.g.* Mars; identification of secondary minerals, clays, state of carbonaceous matter, hydrated crystals. Further benefits to use Raman spectroscopy in meteorites that suffered strong extraterrestrial impacts, allow to evaluate the level of shock by means of the identification of polymorphic minerals characteristic of ultrahigh pressure that can mainly be located in the shock veins such as ringwoodite and majorite polymorphs of olivine and pyroxene among others; in the determination of extraterrestrial aqueous alteration; it is also useful to differentiate by mineralogical identification the SNC meteorites with terrestrial igneous rocks as examples among others. (Miyamoto & Oshumi *et al.*, 1995; Chen *et al.* 2004; Rull *et al.* 2004).

In this paper we combine Raman spectroscopy and Multivariate analysis to implement a reliable, non-destructive method for the authentication of non-metallic meteorites. With this goal, in Section 2 we briefly describe the methodology and materials used to propose this non-destructive technique. In Section 3, we present and discuss our results. Finally, in Section 4 we give our conclusions.

SAMPLES AND METHODS

Real meteorites and meteorite-like rocks were analyzed and used to develop a methodology addressed to identify and classify rocky samples as real meteorite or terrestrial rocks.

Meteorites sample

For this study a thirteen meteorites sample (MS) was analyzed, which includes almost all the metamorphic classes: Esquel (MS-I; mesosiderite), Big rock Donga (MS-II; chondrite), Kilabo (MS-III; chondrite), Ghubara (MS-IV; chondrite), Moss, Ostfold (MS-V; carbonaceous chondrite), Allende (MS-VI; carbonaceous chondrite), Dar al Gani (MS-VII), Estherville (MS-VIII; mesosiderite), Northwest Africa 7936 (MS-IX; chondrite), Vaca Muerta (MS-X; mesosiderite), Al Haggounia (MS-XI; chondrite), Chelyabinsk (MS-XII; chondrite) and Mount Egerton (MS-XIII; achondrite). The meteorite sample was obtained from a recognized source (www.meteoritmarket.com) whose managers belong to the Meteoritical Society, the Geological Society of America and the American Institute of Professional Geologists and certify their meteorites according to the guidelines of the Meteoritical Bulletin Database. Appendix A, at the end of this article, describes with more detail the main reported characteristics of these meteorites.

Terrestrial rocks like meteorites

A group of nine terrestrial rocks (TR) were donated as potential meteorites by different non-certified sources, *i.e.*, amateur collectors, according with their personal criteria of morphology and physical appearance, possible presence of chondrules-spherical grains, regmaglypts and rust coming from oxidized iron, which are characteristics shared by real meteorites. Donors considered these rocks as potential meteorites since they have no visible amounts of quartz, or bubbles and they do not possess a look like river cobbles. The rocks were collected at Concepción del Oro, Zacatecas and Zona del Silencio, which is a desert area located in the central part of the Mapimí Basin, between the states of Chihuahua, Coahuila and Durango. These rocks, however, have never been tested, analyzed or certified as meteorites. We will name this group as TR-I to TR-IX.

Raman spectroscopy

The analysis was performed at the Raman Spectroscopy Laboratory at the Center for Research in Optics, Aguascalientes. The Raman spectra of the meteorite and terrestrial rocks were measured by placing them onto an aluminum substrate and then under a Leica microscope (DMLM) integrated to the Raman system (Renishaw 1000B). In order to retain the most important spectral information from each sample, multiple measurements were conducted in different microscopic points of the sample by moving the substrate on an X-Y stage. The Raman system was calibrated with the first order phonon of silicon at 520 cm^{-1} , by using a silicon semiconductor wafer, and further improved using samples of chloroform (CHCl_3) with bands at 261 , 364 and 667 cm^{-1} and cyclohexane (C_6H_{12}) with bands at 383 , 426 , 801 , 1028 , 1157 , 1265 , 1347 cm^{-1} and 1443 cm^{-1} . The wavelength of excitation was 830 nm and the laser beam was focused (spot size of approximately $2.0\text{ }\mu\text{m}$) on the surface of the sample with a $50\times$

objective. The laser power irradiation over the samples was 45 mW . A total of 180 Raman spectra were acquired from 22 samples (13 meteorites and 9 terrestrial rocks). Each spectrum was collected in the spectral range from $1800\text{--}200\text{ cm}^{-1}$, with an exposure time of 30 secs and a spectral resolution of 2 cm^{-1} .

Data Analysis

The recorded Raman spectra were collected using GRAMS software (version 3.04, Thermo Fisher Scientific, USA; see GRAMS at the reference list). Multivariate analysis and data preprocessing as baseline correction (BLC), autoscaling (centering and standardization), extended multiplicative scatter correction (MSC) and vector normalization (VN), were performed on the Raman spectra, using The Unscrambler® software (version 9.8, CAMO, Norway). Principal component analysis (PCA) was performed over the preprocessed Raman spectra in order to evaluate the spectral differences among meteorites and terrestrial rocks in the PC space. After that, a PLS model was calibrated, allowing the classification of meteorites and terrestrial.

Methodology: A brief description

PCA is a multivariate technique that operates in an unsupervised manner (each number of the groups under study is not known a priori) and it is used to analyze the inherent structure of the data. PCA reduces the dimensionality of the data set by finding an alternative set of coordinates, the principal components (PCs) rocks (*e.g.*, Martens & Naes 1989; Esbensen 2005). PCs correspond to a linear combination of the original variables, which are orthogonal to each other and designed in such a way that each one successively accounts for the maximum variability of the data set. The first principal component (PC1) accounts for as much of the variability in the data as possible, and each succeeding component accounts for as much of the remaining variability as possible. When PC scores are plotted in any combination of the PCs, they can reveal relationships between samples (grouping). PCA provides insight into which is the percentage of variance explained by each PC and how many PCs should be kept to maintain the maximum information from the original data rocks. In turn, when the PC loadings are plotted as function of the variables, the plot reveals the most important diagnostic variables or regions related with the differences found in the data set.

PLS-DA is a version of PLS in which one or several Y-variables are modeled simultaneously, thus taking advantage of possible correlations or collinearity between Y-variables. The discriminant analysis approach assumes that a sample has to be a member of one of the classes included in the analysis. Each class is represented by an indicator variable, a binary variable with a value equal to 1 for members of the class and 0 for non-members (Martens & Naes 1989). This way, by building a PLS model with indicator variables (Y), it is possible to directly predict the class membership from the X-variables describing any given sample rocks. Thus, the model output corresponds to the predicted value for an unknown sample. A correct prediction should have, ideally, a Y value equal to 1 for the members of the meteorites class and 0 for the non-members (terrestrial rocks). All predicted values are accompanied by statistical parameter such as coefficient of determination, R-square, RMSEP, and bias, which counts for the reliability of the prediction.

An average of eight Raman spectra were collected from different superficial zones for each sample in order to obtain a general overview of the chemical composition of each sample. The 180 spectra collected were analyzed in an unsupervised manner by using principal component analysis (PCA), with the objective to evaluate the correlation between the spectral variations and the class of the sample. In this

stage, the scores and loadings were analyzed with the aim to identify groupings correlated with the identity of the samples and, at the same time, identify the influent spectral regions for discrimination purposes.

Afterwards, a classification model was calibrated by using a supervised methodology such as partial least square-discriminant analysis (PLS-DA). The model was calibrated using the 50% of the collected spectra for each sample, and then, validated using the rest of them (test set). Specificity and sensitivity values were computed in order to evaluate the reliability of the calibrated model.

RESULTS AND DISCUSSION

Raman spectra of samples

Figure 1a and 1b depict the average Raman spectra for the TR and MS samples analyzed. As can be observed spectra belonging to TR (Figure 1a), exhibit a great similarity among them, with the main contribution in the spectra of five bands located at *ca.* 225, 290, 410, 495 and 610 cm^{-1} , ascribed to A_{1g} and E_g modes of hematite ($\alpha\text{-Fe}_2\text{O}_3$) at room temperature (de Faria *et al.* 1997). On the other hand, the spectra belonging to MS samples, show diverse spectral patterns, mainly ascribed to olivine bands located at *ca.* 814, 846 and 910 cm^{-1} , pyroxene bands at *ca.* 330, 668 and 1001 cm^{-1} , magnetite and carbon structures, in full agreement with previous determinations (Wang *et al.*, 2004; Rull *et al.*, 2004; Wesełucha-Birczyńska & Żmudzka 2008; Dyar *et al.*, 2011). Magnetite has observable bands at *ca.* 550 and 670 cm^{-1} (Shebanova & Lazor 2003). Amorphous carbon structures (*i.e.*, graphite, microcrystalline graphite) show two well-known bands centered at *ca.* 1288 (D-line) and 1595 cm^{-1} (G-line), being the last one affected for the energy of excitation and crystalline structure, causing some shifts to low energies, also reported by Pócsik *et al.* (1998). The presence of all these components have been reported previously in the literature as principal components of this type of meteorites by Wesełucha-Birczyńska & Żmudzka (2008) and Unsala *et al.* (2012) and among others.

Under the light of these observations, we infer that presence of hematite can be considered as a discriminant factor to establish the identity of a rocky material as terrestrial rock (TR) or not. However,

because to the huge amount of chemical and structural information that can be obtained from vibrational spectra, and the great quantity of spectra that can be obtained in a screening procedure, statistical methods become an indispensable tool to establish the rules for discrimination between MS and TR samples in a reliable way.

Multivariate analysis

We propose a methodology based on non-supervised and supervised multivariate methods such as PCA and PLS-DA, respectively, in order to elucidate the authenticity of meteorites by analyzing the information contained in their vibrational spectra. For this purpose, 180 pre-processed Raman spectra, collected from our TR and MS samples were analyzed firstly by means of principal component analysis (PCA), and subsequently by PLS-DA.

Principal Component Analysis

PCA was conducted over the 180 pre-processed Raman spectra collected from our meteorites (MS) and terrestrial rocks (TR) (90 spectra from MS and 90 from TR) on the spectral range from 1800 to 200 cm^{-1} . The main objective in this stage was to elucidate, in a non-supervised way the inherent structure of the data set according with their spectral differences. In order to do this, PCA-Scores and loadings were analyzed.

Therefore, when scores values of the first three components were plotted, it was possible to observe on a three-dimensional scatter plot a clear discrimination between both types of samples (TR and MS), as shown in Figure 2a, 2b, and 2c at three different views. When these PC's are analyzed altogether, they explain the 64% of the total variance of data set. This fact indicates that data structure is highly related with the chemical composition and structural differences between TR and MS. In these three views of PCA-scores, contrary to the well-defined grouping observed for TR (black spheres), the cluster of meteorites (red spheres) shows sub-groupings along PC2-axis, as indicated for the asterisks in Figure 2c. This behavior indicates that, besides discrimination between rocks and meteorites, it is also possible to get a sub-classification of meteorites according with their main composition (*i.e.*, olivine, pyroxene, magnetite and amorphous carbon). In this case, when we analyze the main difference

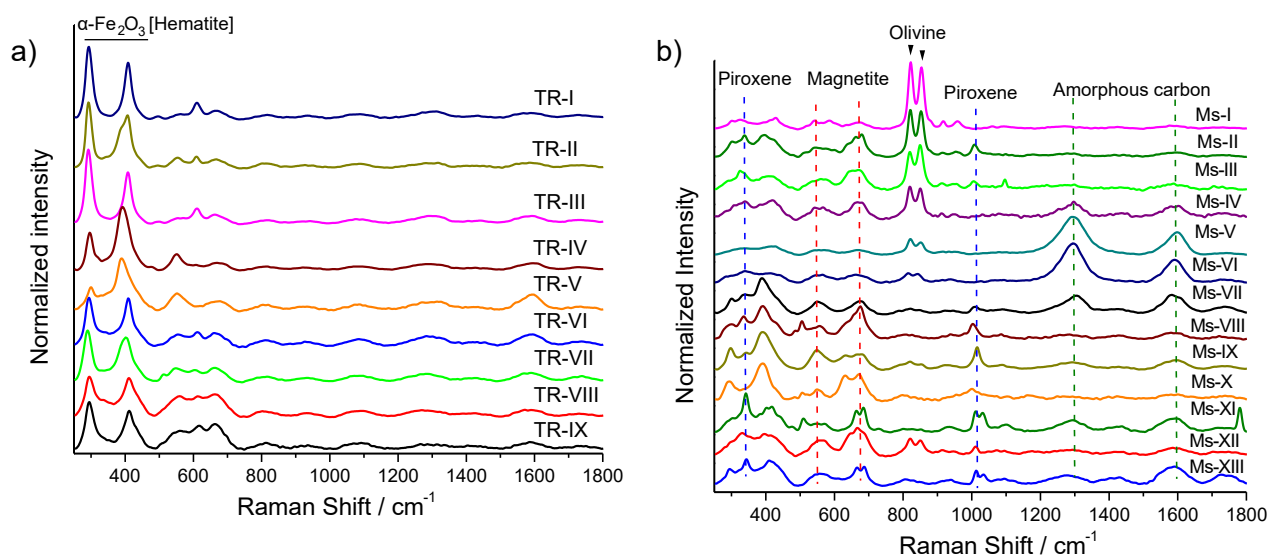


Figure 1. a) Raman spectra of terrestrial rocks (TR-I to TR-IX) which show as their principal characteristic, the bands ascribed to hematite in the range from 250 to 500 cm^{-1} . b) Raman spectra collected from meteorites show bands mainly ascribed to olivine, pyroxene, magnetite and carbonaceous structures (*i.e.* graphite, microcrystalline graphite). Vertical dashed lines on (b) show the main peaks ascribed to the components described in the top.

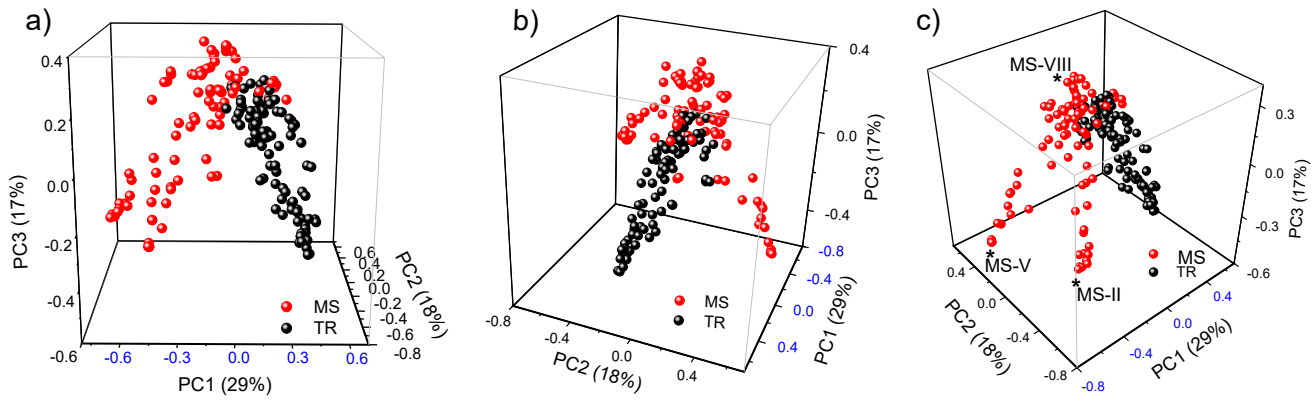


Figure 2. Three different views of the 3D PCA-Scores plots for the Raman spectra collected from TR (black circles) and MS (red circles). The graphs show a clear discrimination between TR and MS samples. Asterisk depicted on plot c) indicate three extreme samples belonging to MS-II, MS-V and MS-VIII samples, with sub-groupings which are strongly correlated with the meteorite composition.

between spectra belonging to these two extreme sub-groups, we could observe that this sub-grouping obeys to the presence or absence of olivine as well as the presence of amorphous carbon (See spectra MS-II and MS-V in Figure 1). In addition, spectra located in the top of the 3D-scores plot (PC3-axis) showed bands ascribed to pyroxene and magnetite as their main features, contrary to those spectra in the bottom of axis where olivine and/or amorphous carbon are the main components of the MS (See spectra MS-VIII in the Figure 1).

In order to identify the most influent variables associated with the discrimination of samples (spectral regions), the loadings values belonging to PC1, PC2 & PC3 were analyzed (see Figure 3a and 3b). Figure 3a depict, enclosed in black frames, the most influent/important spectral regions associated with the discrimination between TR and MS observed in the score plots (Figure 1). These regions are selected in accordance with the highest loadings values, also enclosed in red frames in loadings plots showed in Figure 2b. These regions can be identified in Figure 2b, named and ranged as follow: *i*) region I (R-I),

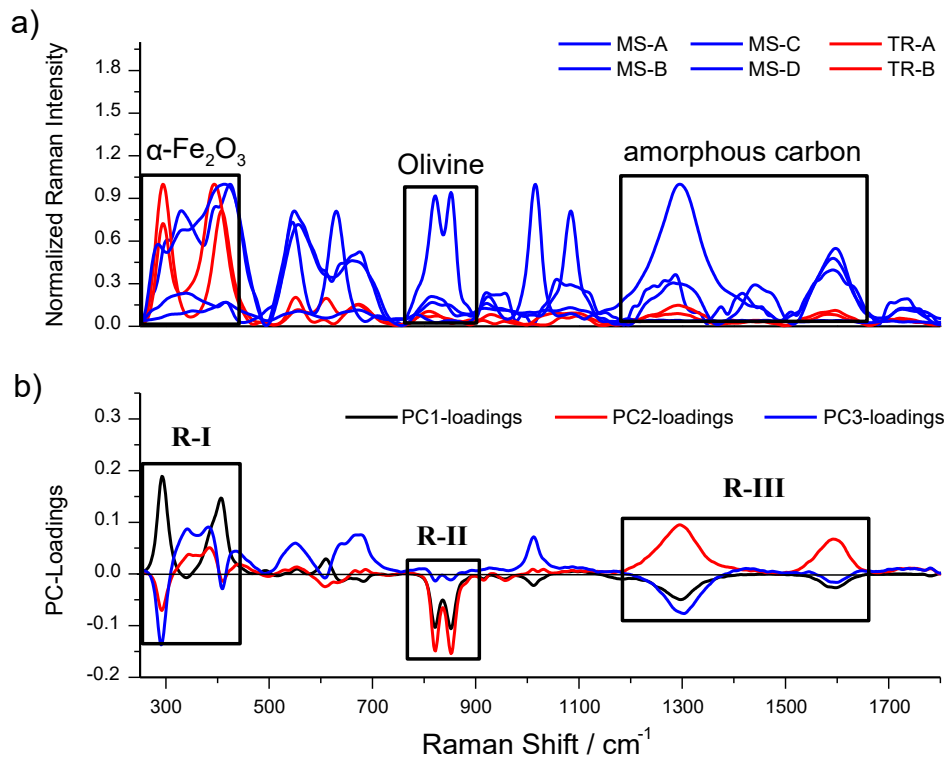


Figure 3. Frame a) depicts six selected spectra showing the main spectral features for MS (blue line) and TR (red line) samples. b) Shows the PCA-loadings plots for three first PC's used to construct the 3D-scores plot. Enclosed in black frames we can appreciate the most influent spectral regions labeled as R-I, R-II and R-III, related with the discrimination between MS and TR. As can be observed, R-I enclose the hematite region, R-II enclose the most representative bands ascribed to olivine, and R-III enclose the D and G bands ascribed to amorphous structures of carbon.

from 250 to 440 cm^{-1} ; *ii*) region II (R-II), from 760 to 910 cm^{-1} ; and *iii*) region III (R-III), from 1190 to 1660 cm^{-1} .

When loadings are analyzed in conjunction with the spectra, it is possible to understand which are the most influent factors associated with the groupings observed in the scores plot. In this address, the highest loadings values observed on R-I can be associated with the presence of hematite in the samples, being this, the main discriminant factor between TR and MS samples. Furthermore, loadings belonging to R-II and R-III can be correlated mainly with the presence of olivine and carbonaceous structures in the MS samples.

Partial least square-discriminant analysis

Once determined the existence of a strong relationship between the spectral features and the identity of our samples from PCA results, a classification model was calibrated by means of PLS-DA method using the information of whole spectral range collected.

In order to calibrate and validate this model, the spectral data set was divided/splatted randomly in two equal independent data sets, one used to build the classification model (calibration stage), and other to validate the model (validation stage). The number of spectra in each data set was selected in order to have an equilibrated statistical weight for calibration and validation stages (Martens & Naes 1989; Esbensen 2005). For this analysis, two classes were defined for the calibration stage, giving a numerical value (*i.e.*, also named dummy variables) to each class as follows; 0 for TR and 1 for MS. Thus, following this criterion, a correct classification for TR samples should have, ideally, a Y-value equal to 0, whereas a value of 1 should be obtained for MS samples. A decision line was fixed at a Y-value of 0.5, and defines whether a sample belongs or not to a particular class. Table 1, shows the statistical values and parameters used for the calibration and validation stages. In addition, the sensitivity and specificity values for the model were computed and showed in Table 2. For the calculation of sensitivity and specificity values, MS and TR samples were defined as “positives” and “negatives” samples, respectively. Samples crossing the decision line were considered as “false positives” or “false negatives”.

Figure 4 depicts the classification plot for the validation set. Horizontal dashed lines correspond to the ideal reference value; 1 for meteorites and 0 for terrestrial rocks. The blue solid line corresponds to the decision line, as described above. From these results, we can point out the feasibility to classify and/or authenticate in a very reliable way, authentic meteorites from terrestrial rocks-like meteorites using

Table 1. Statistical values and parameters of calibration, and validation stage of PLS-DA model in the selected spectral range. ¹Root mean square of calibration/prediction; ²Standard error of calibration/prediction. ^aBaseline correction; ^bExtended multiplicative scatter correction; ^cVector normalization.

Parameters	250–1800 cm^{-1}	
	Calibration	Validation
No. Samples	90	90
PLS-factors	5	5
Math. treatment	raw	raw
Pre-processing	BL ^a , EMSC ^b , VN ^c	BL, EMSC, VN
Calibration outliers	0	-
Correlation	0.92	0.84
R-square	0.85	0.69
RMSEC/RMSEP ¹	0.18	0.27
SEC/SEP ²	0.18	0.27
Bias	3.17E-08	0.049

Table 2. Values of sensitivity and specificity calculated for the calibrated model.

Parameters	% value
Sensitivity (%)	93.0
Specificity (%)	90.0

their spectral signatures, showing a high correlation value of 0.84 for the classification and sensitivity and specificity values of 93 % and 90 %, respectively.

CONCLUSIONS

A methodology based in the use of Raman spectroscopy and chemometrics was developed with the aim of screening and authentication of non-metallic meteorites, in a reliable way. According with the results obtained from principal component analysis, it was possible to identify the existence of a high correlation between the spectral features of both types of samples and their identity (meteorite or terrestrial rock). Furthermore, it was possible to establish by analyzing the PCA-loadings values, that hematite as the main discriminant factor to differentiate TR from MS. On the other hand, olivine, pyroxene, magnetite and the presence of amorphous carbon, graphite and microcrystalline graphite, the most recognized components in our meteorite samples, however, according with the loadings analysis, olivine and the presence of carbonaceous structures were the main signatures for the authentication of our meteorites. The signature of the presence of carbonaceous structures is especially for carbonaceous meteorites.

Furthermore, the model calibrated for the authentication of meteorites by means of PLS-DA showed sturdy statistical values, allowing a correct classification of our test set with sensitivity and specificity percentage values of 93 % and 90 %, respectively. This fact indicates that the model calibrated is able to distinguish in a very reliable way, rocky samples as authentic meteorites or terrestrial rocks.

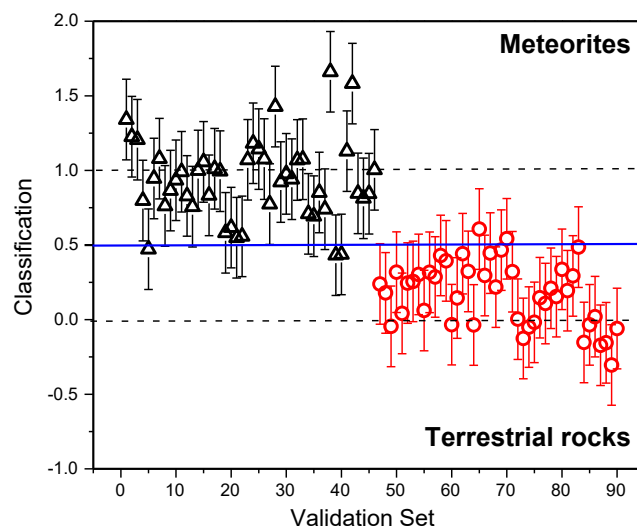


Figure 4. Classification of the validation set. ○ (empty red circle) corresponds to terrestrial rocks samples, and Δ (empty black triangle) to authentic meteorite samples. Error bars corresponds to RMSEP value.

Finally, the results obtained in this work show the feasibility of use this methodology based on Raman spectroscopy and chemometrics with the screening purposes for the reliable authentication of stony meteorites, in a non-destructive and reagent-free way.

Acknowledgements. AGS thanks SNI and CONACYT for grant 245866, and to LERMA at the Observatoire de Paris for a visiting astronomer position during which this work started.

Author contributions. González-Sánchez and C. Araujo-Andrade proposed the project, methodology, investigation, spectra analysis, data processing, multivariate analysis and interpretation, writing, review, editing. Fraustoo-Reyes and Esparza-Ibarra performed the Raman spectroscopy analysis. Gutiérrez-Rodríguez: data processing and interpretation.

Data availability statement. The authors confirm that all data supporting the findings of this study are available in this article.

Declaration of Competing Interests. The authors declare that they are not aware of any financial conflicts of interest or personal relationships that could have influenced the work reported in this article.

Funding. AGS received funding by the former CONACYT under grant 245866, through a sabbatical year.

REFERENCES

- Anderson, S., Towner, M., Bland, P., Haikings, C., Volante, W., Sansom, E., Devillepoix, H., Shober, P., Hartig, B., Cupak, M., Jansen-Sturgeon, T., Howie, R., Benedix, G., & Deacon, G. (2020). Machine learning for semi-automated meteorite recovery. *Meteoritics & Planetary Science*, 55(11), 2461–2471. doi: 10.1111/maps.13593
- Anderson S. L., Towner, M. C., Fairweather, J., Bland, P. A., Devillepoix, H. A. R., Sansom, E. K., Cupák, M., Shober, P. M., & Benedix, G. K., (2022). Successful Recovery of an Observed Meteorite Fall Using Drones and Machine Learning. *The Astrophysics Journal Letters*, 930(2), L25. DOI 10.3847/2041-8213/ac66d4
- Andrews, S. M. (2020). Observations of Protoplanetary Disk Structures. *Annual Review of Astronomy and Astrophysics*, 58, 483–528. <https://doi.org/10.1146/annurev-astro-031220-010302>
- ARES project: Astro Material Research and Exploration Science, (2023). *Meteorite Falls*, National Aeronautic and Space Administration. <https://ares.jsc.nasa.gov/meteorite-falls/>
- Bally, J. & Devine, D. (1994). A Parsec-Scale “Superjet” and Quasi-periodic Structure in the HH 34 Outflow?. *The Astrophysical Journal*, 428, L65–L68.
- Bast, J. E., Brown, J. M., Herczeg, G. J., van Dishoeck, E. F., & Pontoppidan, K. M., (2011). Single peaked CO emission line profiles from the inner regions of protoplanetary disks. *Astronomy & Astrophysics*, 527, A119. <https://doi.org/10.1051/0004-6361/201015225>
- Benisty, M., Dominik, C., Follette, C., Garufi, A., Ginski, C., Hashimoto, J., Keppler, M., Kley, W., Monnier, J. (2022). Optical and Near-infrared View of Planet-forming Disks and Protoplanets, arXiv:2203.09991v1 [astro-ph.EP]. <https://doi.org/10.48550/arXiv.2203.09991>
- Bland, P.A., Smith, T.B., Jul, A.J.T., Berry, F. J., Bevan, A. W. R., Cloudt, S., & Pillinger, C. T. (1996). The flux of meteorites to the Earth over the last 50 000 years. *Monthly Notices of the Royal Astronomical Society*, 283(2), 551–565. <https://doi.org/10.1093/mnras/283.2.551>
- Campbell-Brown, M. D., & Hildebrandt, A. (2004). A new analysis of fireball data from the meteorite observation and recovery Project (MORP). *Earth, Moon and Planets*, 95, 1–4, 489. <https://doi.org/10.1007/s11038-005-0664-9>
- Chen, M., El Goresy, A., & Gillet, P. (2004). Ringwoodite lamellae in olivine: Clues to olivine–ringwoodite phase transition mechanisms in shocked meteorites and subducting slabs. *Proceedings of the National Academy of Sciences, USA*, 101(42), 15033–15037. <https://doi.org/10.1073/pnas.040504810>
- Colas, F. (2020). FRIPON: a worldwide network to track incoming meteorites. *Astronomy and Astrophysics*, 644, A53. <https://doi.org/10.1051/0004-6361/202038649>
- Cieza, L. A. (2015). The Structure and Evolution of Protoplanetary Disks: an infrared and submillimeter view. In J. H., Kastner, B., Stelzer, S., Metchev (Ed.), *Young Stars & Planets Near the Sun, Proceedings IAU Symposium No. 314*.
- Citron, R.I., Jenniskens, P., Watkins, C., Sinha, S., Shah, A., Raissi, C., Devillepoix, H., & Albers, J. (2021). Recovery of meteorites using an autonomous drone and machine learning. *Meteoritic and Planetary Sciences*, 56(6) 1073–1085. <https://doi.org/10.1111/maps.13663>
- De Faria, D. L. A., Venâncio-Silva, S. & de Oliveira, M. T. J. (1997). Raman microspectroscopy of some iron oxides and oxyhydroxides. *Journal of Raman Spectroscopy*, 28, 873–878. [https://doi.org/10.1002/\(SICI\)1097-4555\(199711\)28:11<873::AID-JRS177>3.0.CO;2-B](https://doi.org/10.1002/(SICI)1097-4555(199711)28:11<873::AID-JRS177>3.0.CO;2-B)
- De Leon J., Takami, M., Karr, J.M., et al. (2015). Near-IR High-resolution imaging polarimetry of the SU Aur disk: clues for tidal tails?. *The Astrophysical Journal Letters*, 806, L10. doi:10.1088/2041-8205/806/1/L10
- Dobričá, E., Engrand, C., Quirico, E., Montagnac, G., & Duprat, J. (2011). Raman characterization of carbonaceous matter in CONCORDIA Antarctic micrometeorites. *Meteoritics & Planetary Science* 46(9), 1363–1375. <https://doi.org/10.1111/j.1945-5100.2011.01235.x>
- Donaldson H. K. L., Wyatt, M. B., Helbert, J., Maturilli, A., & Pieters, C.M. (2009). Constraining lunar surface mineralogy with combined thermal and near infrared spectral data. *Proceedings Lunar and Planetary Science Conference*, 40th, 2286.
- Donato, T.P., Nascimento-Dias, B.L. & Zucolotto, M.E. (2023). Application of Raman spectroscopy in the identification of carbonaceous materials in the carbonaceous chondrite Allende. III Congreso Latinoamericano de Astrobiología 2021. *Revista Mexicana de Astronomía y Astrofísica, Serie de Conferencias*, 55, 74–76.
- Dong, R., Liu, S.-Y., & Fung, J. (2023). Observational Signatures of Planets in Protoplanetary Disks: Planet-induced Line Broadening in Gaps. *The Astrophysical Journal*, 870(2), 72. DOI 10.3847/1538-4357/aaf38e
- DOMe Project: Detection and Observation of Meteorites, (2022). *Blog, Espace Pour la Vie Montreal*. <https://m.espacepourlavie.ca/blogue/en/lookout-meteorites-dome-project>
- Dudorov, A. e. & Eretnova, O. V. (2020). The rate of falls of meteorites and bolids. *Solar System Research*, 54, 223–235. <https://doi.org/10.1134/S003809462003003X>
- Dyar, M. D., Glotch, T.D. M.D., Wopenka, L.B., Tucker, J.M., Seaman, S.J., Marchand, G.J., Klima, R., Hiroi, T., Bishop, J.L., Pieters, C., & Sunshine, J. (2011). Spectroscopy of Yamato 984028. *Polar Science*, 4, 530–549.
- Edwards, S., Cabrit, S., Strom, S. E., Heyer, I., Strom, K. M., Anderson, E. (1987). Forbidden Line and H alpha Profiles in T Tauri Star Spectra: A Probe of Anisotropic Mass Outflows and Circumstellar Disks. *The Astrophysical Journal*, 321, 473. DOI: 10.1086/165646
- Esbensen, K. H. (2005). *Multivariate Data Analysis - In Practice*. Fifth ed., CAMO Process AS, Esbjerg, Denmark.
- Flores-Gutiérrez, D., Urrutia-Fucugauchi, J., Pérez-Cruz, L., Díaz-Hernández, R., & Linares-López, C. (2010). Micromagnetic and microstructural analysis in chondrules of the Allende meteorite. *Revista Mexicana de Ciencias Geológicas*, 27(2), 162–174.
- Fries, M. & Fries, J. (2010). Doppler weather radar as a meteorite recovery tool. *Meteoritics and Planetary Sciences*, 45, 1476–1487.
- Goldstein, J.I. & Ogilvie, R.E. (1965). The growth of Widmanstätten pattern in metallic meteorites. *Geochimica and Cosmochimica Acta*, 29, 893–920.
- GRAMS, (2010). *Spectroscopy Software*, 3.04, Thermo Fisher Scientific. <https://www.thermofisher.com/order/catalog/product/INF-15000>
- Greenhagen, B., Lucey, P., Wyatt, M. B., Gloth, T. D., Alleb, C., Arnold, J., Banfield, J., Bowles, Donaldson, K., Hayne, P. O., Song, E., Thomas, I., & Paige, D. (2010). Global silicate mineralogy of the Moon from the Diviner lunar radiometer. *Science*, 329 (5998), 1507–1509. DOI 10.1126/science.1192196
- Hankey, M., Fries, M., Matson, R., Fries, J. (2017). Automated Detection of Meteorite Strewfields in Doppler Weather Radar. *Planetary and Space Science*, 143, 199–202, doi: 10.1016/j.pss.2017.02.008
- Hochleitner, R., Tarcea, N., Simon, G., Kiefer, W., & Popp, J. (2004). Micro-Raman spectroscopy: a valuable tool for the investigation of extraterrestrial materia. *Journal of Raman Spectroscopy*, 35, 9, 515–518. <https://doi.org/10.1002/jrs.1190>

- Huidobro, J., Aramendia, J., García-Florentino, C., Ruiz-Galende, P., Torreflez, I., Castro, K., Arana, G., Madariaga, J. M. (2021). Mineralogy of the RBT 04262 Martian meteorite as determined by micro-Raman and micro-X-ray fluorescence spectroscopies. *Journal of Raman Spectroscopy*, 53(3), 323–676. <https://doi.org/10.1002/jrs.6291>
- Hutchinson, I. B., Ingle, R., Edwards, H. G.M., McHugh, M., Malherbe, C., Parnell, J. (2014). Raman spectroscopy on Mars identification of geological and bio geological signatures in Martian analogues using miniaturized Raman spectrometers. *Philosophical Transactions of the Royal Society A, Mathematical, Physical and Engineering Sciences*, A372:20140204. <http://dx.doi.org/10.1098/rsta.2014.0204>
- Ishiguro, M. (2008). Cometary dust trail associated with Rosetta mission target: 67P/Churyumov–Gerasimenko. *Icarus*, 193, 1, 96–104. <https://doi.org/10.1016/j.icarus.2007.08.027>
- Ismailov, N. Z., Valiev, U. S. & Dzhililov, N. S. (2022). Protoplanetary Disks around Classical T Tauri Stars. *Odessa Astronomical Publications*, 35, 30–40. DOI: 10.18524/1810-4215.2022.35.268006
- Jensen, E. L., & Akeson, R. (2014). Misaligned protoplanetary disks in a young binary star system. *Nature*, 511, 567–569. <https://doi.org/10.1038/nature13521>
- Krot, A. N., Yurimoto, H., Hutcheon, I. D., Libourel, G., Chaussidon, M., Tissandier, L., Petaev, M.I., MacPherson, G. J., & Paque-Heather, J. (2007). Remelting of refractory inclusions in the chondrule-forming regions: Evidence from chondrule-bearing type C calcium-aluminum-rich inclusions from Allende. *Meteoritics and Planetary Sciences*, 42(7/8), 1197–1219. <https://doi.org/10.1111/j.1945-5100.2007.tb00569.x>
- Malarewicz, V., Beyssac, O., Zanda, B., Hewins, R., Pont, S., Bouley, S., Bernard, S., Gauthier, M., Morand, M., Garino, Y., Rosier, P. (2023). Raman spectroscopy investigations of the Martian regolith breccia Northwest Africa 7533: A support to in situ Raman spectroscopy on Mars. *J. Raman Spectroscopy*, 54 (7), 748–768. <https://doi.org/10.1002/jrs.6556>
- Martens, H. & Næs, T. (1989). *Methods for calibration, in Multivariate Calibration*. Wiley, Chichester, England.
- Matzner, C. D., & McKee, C. F. (2000). Efficiencies of Low-Mass Star and Star Cluster Formation. *The Astrophys. Journal*, 545, 364–378. DOI 10.1086/317785
- McSween, H. Y. Jr. (1977). *Chemical analyses of chondrules and inclusions in Chondritic Meteorites-A Tabulation*. Department of Geological Sciences, Harvard University and Center for Astrophysics, Cambridge, Mass.
- Milley, E.P., Hawkers, R. & Ehrman, J. M. (2007). Meteor luminosity simulation through laser ablation of meteorites. *Monthly Notices of the Royal Astronomical Society: Letters*, 382(1), L67–L71. DOI:10.1111/j.1745-3933.2007.00390.x
- Miyamoto, M. & Oshumi, K. (1995). Micro Raman spectroscopy of olivines in L6 chondrites: Evaluation of the degree of shock. *Geophysical Research Letters*, 22(4), 437–440. <https://doi.org/10.1029/94GL03281>
- Montmerle, T., Augereau, J. C., Chaussidon, M., Gounelle, M., Marty, B., & Morbidelli, A. (2006). Solar System Formation and Early Evolution: the First 100 Million Years. In M., Gargaud, et al. (Ed.), *From Suns to Life: A Chronological Approach to the History of Life on Earth*. Springer, New York, NY. https://doi.org/10.1007/978-0-387-45083-4_3
- Musa, M., Rossini, R., Di Martino, D., Riccardi, M. P., Clemenza, M., & Gorini, G. (2021). Combining Micro-Raman Spectroscopy and Scanning Electron Microscopy Mapping: A Stony Meteorite Study. *Materials (Basel)*, 14(24): 7585. <https://doi.org/10.3390/ma14247585>
- Nascimento-Dias, B. L., Donato, T. P., Zucolotto, M. E., & Anjos, V. (2021). Overview about Raman spectroscopy of types of olivine group minerals: A brief review. *Journal of Raman Spectroscopy*, 53(11), 1942–1946. <https://doi.org/10.1002/jrs.6412>
- Oberst, J., Heinlein, D., Kholer, U., & Spurny, P. (2004). The multiple meteorite fall of Neuschwanstein: Circumstances of the event and meteorite search campaigns. *Meteoritic and Planetary Science*, 39(10), 1627–1641. <https://doi.org/10.1111/j.1945-5100.2004.tb00062.x>
- Pilkington, M., & Grieve, R. A. F. (1992). The Geophysical Signature of Terrestrial Impact Craters. *Reviews of Geophysics*, 30(2), 161–181. <https://doi.org/10.1029/92RG00192>
- Pócsik, I., Hundhausen, M., Koós, M., & Ley, L. (1998). Origin of the D peak in the Raman spectrum of microcrystalline graphite. *Journal of Non-Crystalline Solids*, 227–230, Part 2, 1083–1086. [https://doi.org/10.1016/S0022-3093\(98\)00349-4](https://doi.org/10.1016/S0022-3093(98)00349-4)
- Ray, T. P. & Ferreira, J. (2021). Jets from young stars. *New Astronomy Reviews*, 93, 101615. <https://doi.org/10.1016/j.newar.2021.101615>
- Reipurth, B., Yu, K. C., Rodriguez, L. F., Heathcote, S., Bally, J., (1999). Multiplicity of the HH 111 jet source: it Hubble Space Telescope NICMOS images and VLA maps. *Astronomy and Astrophysics*, 352, L83–L86.
- Reipurth, B., Yu, K. C., Heathcote, S., Bally, J., Rodriguez, L. F., (2000). Hubble Space Telescope NICMOS Images of Herbig-Haro Energy Sources: [Fe II] Jets, Binariness, and Envelope Cavities *The Astronomical Journal*, 120(3), 1449–1466. DOI 10.1086/301510
- Rodríguez, L. F., & Reipurth, B. (1994). The exciting source of the Herbig-Haro 111 jet complex : VLA detection of a one-sided radio jet. *Astronomy and Astrophysics*, 281, 882–888.
- Rull, F., Martínez-Frías, J., Sansano, A., Medina, J. & Edwards, H.G.M. (2004). Comparative micro-Raman study of the Nakhla and Vaca Muerta meteorites. *J. Raman Spectrosc.*, 35: 497-503. <https://doi.org/10.1002/jrs.1177>
- SAMBA project: Search for Antarctic Meteorites, (2010). http://www.antarcticstation.org/science_projects/detail/samba_collecting_meteorites_in_antarctica
- Scott, E. R. D. (2007). Chondrites and the Planetary Disk. *Annual Review of Earth and Planetary Sciences*, 35, 577–620. <https://doi.org/10.1146/annurev.earth.35.031306.140100>
- Shebanova, O. N. & Lazor, P. (2003). Raman spectroscopic study of magnetite (Fe₃O₄): a new assignment for the vibrational spectrum. *Journal of Solid State Chemistry*, 174(2), 424–430. [https://doi.org/10.1016/S0022-4596\(03\)00294-9](https://doi.org/10.1016/S0022-4596(03)00294-9)
- Steele, A., Fries, M. D., & Amundsen, H. E. F. (2007). Comprehensive imaging and Raman spectroscopy of carbonate globules from Martian meteorite ALH 84001 and a terrestrial analogue from Svalbard. *Meteoritics & Planetary Science*, 42(9), 1549–1566. <https://doi.org/10.1111/j.1945-5100.2007.tb00590.x>
- Stephan, T., Jessberger, E. K., Klock, W., Rulle, H., & Zehnpfenning, J. (1994). Isotope systematics and shock-wave metamorphism: III. K-Ar in experimentally and naturally shocked rocks; the Haughton impact structure, Canada. *Earth and Planetary Science Letters*, 129(3–4), 453–467. [https://doi.org/10.1016/0016-7037\(92\)90227-A](https://doi.org/10.1016/0016-7037(92)90227-A)
- Strom, K. M., Strom, S. E., Edwards, S., Cabrit, S., & Skrutskie, M. (1989). Circumstellar material associated with Solar-type pre-main-sequence stars: A possible constraint of the timescale for planet forming. *The Astronomical Journal*, 97, 1451. DOI 10.1086/115085
- Sturm, J. A., McClure, M. K., Law, C. J. et al. (2023). The edge-on protoplanetary disk HH 48 NE. *Astronomy & Astrophysics*, 667, A17. <https://doi.org/10.1051/0004-6361/202346052>
- Takami, M., Karr, J. L., Hashimoto, J. et al. (2023). High-contrast near infrared imaging polarimetry of the protoplanetary disk around RY Tau. *The Astrophysical Journal*, 772(2), 145 <https://doi.org/10.1088/0004-637X/772/2/145>
- Unsalan, O., Yilmazb, A., Bolukbasib, O., Ozturkc, B., Esenoglu, H.H., Ildiz, G.O. & Ornek, C.Y. (2012). Micro-Raman, FTIR, SEM-EDX and structural analysis of the Çanakale meteorite. *Spectrochimica Acta Part A*, 92, 250– 255. <https://doi.org/10.1016/j.saa.2012.02.014>
- Unscrambler® (2012). Software version 9.8, CAMO Software AS, Trondheim, Norway. <https://docaic.rstools.csic.es/es/software/Unscrambler>
- Wang, A., Kuebler, K., Jolliff, B., & Haskin, L. (2004). Mineralogy of a Martian meteorite as determined by Raman spectroscopy. *Journal of Raman Spectroscopy*, 35(6), 504. <https://doi.org/10.1002/jrs.1175>
- Wang, H., Xin, Y., Fang, P., Wang, Y., Duan, M., Wu, W., Yang, R., Liu, S., Zhang, L., & Wan, X. (2023). Quantitative Analysis of Meteorite Elements Based on the Multidimensional Scaling–Back Propagation Neural Network Algorithm Combined with Raman Mapping-Assisted Micro-Laser Induced Breakdown Spectroscopy. *Chemosensors*, 11(11), 567. <https://doi.org/10.3390/chemosensors11110567>
- Weselucha-Birczyńska, A. & Żmudzka, M. (2008). Micro-Raman spectroscopy characterization of selected meteorites. *Journal of Molecular Structure*, 887(1–3), 253–261. <https://doi.org/10.1016/j.molstruc.2008.01.029>

- Williams, J. P., & Cieza, L. A. (2011). Protoplanetary Disks and Their Evolution. *Annual Review of Astronomy and Astrophysics*, 49, 67–117. <https://doi.org/10.1146/annurev-astro-081710-102548>
- Wolf, S., Gueth, F., Henning, T. & Kley, W. (2002). Detecting Planets in Protoplanetary Disks: A Prospective Study. *The Astrophysical Journal*, 566(2), L97–L99. DOI: 10.1086/339544
- Yang, J., & Goldstein, J. I. (2005). The formation of the Widmanstätten structure in meteorites. *Meteoritics & Planetary Science*, 40(2), 239–253. <https://doi.org/10.1111/j.1945-5100.2005.tb00378.x>
- Zinnecker, H., Krabbe, A., McCaughrean, M. J., Stanke, T., Stecklum, B., Brandner, W., Padgett, D. L., Stapelfeldt, K. R., Yorke, H. W. (1999). A search for Young Solar System Analogues with the VLT. *Astronomy and Astrophysics*, 352, L73–L78
- Zipfel, J., Spettel, B., Palme, H., Wolf, D., Franchi, I., Sexton, A. S., Pillinger, C. T. & Bischoff, A. (1998). Dar Al Gani 400, chemistry and petrology of the largest lunar meteorite. *Meteoritics and Planetary Science*, 33 (Suppl.), A171.

APPENDIX A: Meteorites samples

We list the meteorite samples used for this analysis, providing the most relevant information concerning their morphological and chemical properties. **We state that the description of the meteorites was taken, without changes**, from the Meteoritical Bulletin Database and assigned by the database editor, in agreement to the most recent classification that appears in either the Catalogue of Meteorites, MetBase, the US Antarctic Meteorite Newsletter, the Japanese Meteorite Newsletter, and the Meteoritical Bulletin. The cited mineralogy and petrology are accord with Mineralogy and Petrology 37:157–179 and the American Mineralogist 72:1031–1042; 73; 200.

MS-I) Esquel: This meteorite was found in 1951 near the Patagonian town Esquel, province of Chubut, Argentina. It is a **pallasite** type iron meteorite that contains abundant silicate inclusions in a nickel-iron matrix, shows large olivine (peridot) crystals with some degree of transparency: 8.5 % Ni, 21.5 ppm Ga, 55.5 ppm Ge, 0.023 ppm Ir.

MS-II) Big rock Donga: it was found in 1970 in South Australia, Australia. This meteorite is classified as a **H6 chondrite**. Chondrites of the H group are distinguished by sub-solar Mg/Si and refractory/Si ratios, oxygen isotope compositions that plot above the terrestrial fractionation line, and a large volume percentage of chondrules, with only 10–15 vol. % fine-grained matrix. Type 6 applies to chondrites metamorphosed under conditions sufficient to homogenize all mineral compositions, convert all low-Ca pyroxene to orthopyroxene, coarsen secondary phases such as feldspar to sizes $\geq 50 \mu\text{m}$, and obliterate many chondrule outlines; no melting has occurred. It contains olivine $\text{Fa}_{19,6}$, pyroxene $\text{Fs}_{17,4}$, Wo_3 .

MS-III) Kilabo: The fall of this meteorite was observed in Kilabo, Nigeria in July 2002. It is classified as an ordinary **LL6 chondrite**, because its low iron and low metal content group among the ordinary chondrites. It is distinguished by a low siderophile element content, fairly large chondrules ($\sim 0.9 \text{ mm}$), and oxygen isotope compositions further above the terrestrial fractionation line than those of other ordinary chondrites. It contains Olivine $\text{Fa}_{31,1}$, $\text{CaO} < 0.09$, predominantly < 0.05 . Low Ca-pyroxene, $\text{Fs}_{27,1}$ $\text{PMD} = 0.02$. It is also reported an abundant coarse-grained plagioclase is also reported, mainly $\text{An}_{84}\text{Or}_{15}$, from $\text{An}_{61}\text{Or}_{25}$ to $\text{An}_{86}\text{Or}_3$. Coarse grained diopside and troilite is abundant, pentlandite is a minor phase. The meteorite is highly brecciated and appears to be a polymict regolith breccia in places.

MS-IV) Ghubara: It was found in Oman, Southern Arabia in 1954. This meteorite is classified as a **L5 chondrite** (Xenolithic) petrographic type (Fayalite 24.7 mol %; Ferrosilite 21.4 mol %). It is distinguished by subsolar Mg/Si, oxygen isotope compositions above the terrestrial

fractionation line, and a large percentage of chondrules, with up to 10–15 vol. % fine-grained matrix. The low-iron (L) chemical group of ordinary chondrites, distinguished by their low siderophile element content, moderate sized chondrules (0.7 mm), and oxygen isotope compositions that intermediate between H and LL group ordinary chondrites. Designates chondrites that have been metamorphosed under conditions sufficient to homogenize olivine and pyroxene, convert all low-Ca pyroxene to orthopyroxene, cause the growth of various secondary minerals, and blur chondrule outlines. The major composition of this meteorite is Si (28.3–27.1 %), Fe (22.1–19.8 %), Mg (17.3–15.2 %), Al (2.9–2.4 %), Ca (1.7–1.9 %), and S (1.0–0.97 %).

MS-V) Moss: The fall of this meteorite was observed on July 2006, in Østfold, Norway. It is classified as a **carbonaceous chondrite CO3.6**. The Meteoritical Bulletin Database describe it with an abundant contain of small chondrules (most $< 200 \mu\text{m}$), small ($< 1 \text{ mm}$) amoeboid olivine aggregates (AOAs) and refractory inclusions, as well as isolated grains of olivine, troilite, and kamacite set in a gray matrix. Chondrule types are dominated by type-I PO, with other varieties of type I and II chondrules plus RP, C, and BO. All type I chondrules show diffusional entry of FeO around edges and along cracks of forsterite grains. Olivine histogram is flat, resembling that of Ornans (range $\text{Fa}_{0.3-42}$, average $\text{Fa}_{19.9}$, $\sigma=65\%$, $n=60$); Cr_2O_3 content of fayalitic olivine is low ($0.09 \pm 0.09 \text{ wt. \%}$). Image analysis gives 2.2 vol. % metal and 2.4 vol. % FeS. Refractory inclusions contain spinel, calcic pyroxene, and abundant nepheline that replaces melilite and other primary phases; some perovskite has been transformed to ilmenite. Some AOAs contain relict cores of forsterite, but most of the olivine has been converted to more fayalitic compositions; degree of oxidation of AOAs is similar to type 3.6 CO chondrites such as ALH 77003. Matrix is mildly recrystallized and sulfur-poor; matrix olivine has similar composition to olivine in fine-grained chondrules and inclusions.

MS-VI) Allende: This meteorite fell as a shower of stones in February 1969, in Allende, Chihuahua, México. It is classified as a CV3 **carbonaceous chondrite** which contains 43 % of chondrules, 38.4 % of matrix, 9.4 % of Calcium-Aluminum Inclusions (CAI), 3.2 % of olivine inclusions, 3.1 % of opaque minerals, and 2.9 % of lithic and mineral fragments (Flores-Gutiérrez *et al.* 2010; McSween, 1977). As stated by Scott (2007) and Krot *et al.* (2007) the macroscopic texture of Allende reflects the abundance of chondrules of sub-millimeter size within an aphanitic black matrix. Allende meteorite is part of the oxidized chondrites with an anhydrous mineralogy, with hydrous phases restricted to chondrules and CAIs. Oxidized chondrites show olivine rich in FeO and no iron metal blebs, in contrast to the reduced chondrites.

MS-VII) Dar al Gani: It was found in Dar al Gani in the Lybian Sahara in 1998. The samples of this meteorite are partly covered with a brownish fusion crust; from gray fresh surfaces to dark gray; matrix is well consolidated; clasts include subophitic and fine-grained to microporphyritic impact-melt breccias, granulitic fragments, intergranularly recrystallized anorthosites, and mineral fragments; chemical and O isotope composition is characteristic of lunar highland meteorites (Zipfel *et al.*, 1998). Its minerals are anorthite, olivine, low-Ca pyroxene, more calcic pigeonite, Ti-bearing chromite, ilmenite and troilite. Its geochemistry is mainly: Olivine ($\text{Fa}_{16.0-33.9}$; $\text{FeO/MnO} = 90-108$), low-Ca pyroxene ($\text{Fs}_{29.8-30.3}\text{Wo}_{4.8-6.4}$, $\text{FeO/MnO} = 50-57$), pigeonite ($\text{Fs}_{33.7}\text{Wo}_{10.2}$; $\text{Fs}_{43.6}\text{Wo}_{7.5}$; $\text{FeO/MnO} = 59-61$).

MS-VIII) Estherville: It's fall was observed in the Emmet County, Iowa, USA in 1879. It is classified as a **mesosiderite-A3/4**, *i.e.*, is a complex stony-irons meteorite which is a mixture of nickel-iron and silicates, mainly comprised of olivine and pyroxene. It has experienced strong impacts which have mixed once molten Fe-Ni metal with an assortment of silicate clasts. Several larger mesosiderite finds are known, but weathering creates substantive interpretation problems — especially when trying to determine which sulfides, sulfates and phosphates within an exposed meteoritical mass are pre-terrestrial and by products of exposure to the earth's environment. Estherville's Fe-Ni metal (56 wt. %), with prominent nodules and frequent Widmanstätten patterns provide ample Fe-rich material. Schreibersite, troilite, chromite and other phases account for <5 wt. % of the meteorite.

MS-IX) Northwest Africa 7936: This meteorite was found in 2012 at Northwest, Africa, whose reported classification is as an ordinary chondrite L3. Meteorites of this type These are a low-iron (L) chemical group of ordinary chondrites, distinguished by their relatively low siderophile element content, moderate sized chondrules (~0.7 mm), and oxygen isotope composition intermediate between H and LL group ordinary chondrites. It presents abundant and well formed chondrules, olivine, orthopyroxene, pigeonite, augite, sodic plagioclase, chromite, stained kamacite and troilite. Olivine ($\text{Fa}_{1.4-76.8}$; Cr_2O_3 in ferroan examples is 0.06-0.83 wt. %, mean 0.23 ± 0.22 wt. %, $N = 14$), orthopyroxene ($\text{Fs}_{1.0-43.8}\text{Wo}_{0.9-2.8}$), pigeonite ($\text{Fs}_{18.2}\text{Wo}_{22.1}$), augite ($\text{Fs}_{8.5}\text{Wo}_{41.9}$).

MS-X) Vaca Muerta: Found in 1861 in Vaca Muerta, Atacama, Chile. It is classified as a mesosiderite A1. It is a stony-iron meteorite, with half and half mixture of nickel-iron and rock, with mean composition of the metal is 8.8 % Ni, 9.6ppm Ga, 42.8 % Ge, 2.2 % Ir.

MS-XI) Al Haggounia: It was found in 2006 at Al Haggounia, Morocco. According with the Meteoritical Database the presence of sparse, well-formed enstatite-bearing chondrules containing glass (mostly dissolved) and the lack of recrystallization of the matrix make this an EL3 chondrite. Based upon the replacement of troilite by iron sulfate and complete dissolution of primary metal, the weathering/diagenetic grade is W4. Most stones of this meteorite have exterior light orange staining, and some contain dark brown rinds or cross-cutting veins (1-2 mm wide) of magnetic, fine grained iron oxide and

hydroxide minerals. Relatively fine but variable grain size (0.3 to 1.5 mm), and composed predominantly of prismatic grains of essentially pure enstatite with ~15 vol. % oligoclase, accessory iron sulfate pseudomorphs after troilite (with fresh, subparallel exsolution blades of daubreelite) and sporadic rounded to ellipsoidal grains of graphite (up to 1.2 mm across). Small (0.5 - 1 mm) lobate cavities partly coated with fine grained calcite, halite, gypsum and iron sulfate are present in the interior of even the freshest stones. Small grains found as inclusions within enstatite are fresh Ti-free troilite, pure Mn-alabandite, daubreelite, fresh oldhamite (some Mn-bearing), schreibersite, and very rare specks of kamacite and taenite. Minor barite is present. Its chemical properties include Pyroxene ($\text{En}_{98.4}\text{Wo}_{1.4}$, $\text{Al}_2\text{O}_3 = 0.21$ wt. %), plagioclase ($\text{An}_{13.5-15.3}\text{Or}_{3.0-4.4}$). **Oxygen Isotopes** (D. Rumble, *CIW*): Analyses of two acid-washed whole rock fragments by laser fluorination gave $\delta^{18}\text{O} = 5.50, 5.56$ ‰; $\delta^{17}\text{O} = 2.89, 2.90$ ‰; $\Delta^{17}\text{O} = -0.001, -0.026$ ‰, respectively.

MS-XII) Chelyabinsk: The fall of this this meteorite was observed on February 15, 2013 in parts of the Kurgan, Tyumen, Ekaterinburg and Chelyabinsk districts of Rusia. It is classified as an ordinary chondrite LL5; the interior of the stones is fresh but, in some pieces, there is evidence for weak oxidation of metal grains. The main phases are olivine and orthopyroxene. Olivine shows mosaicism and planar fractures. Rare grains of augite and clinobronzite are present. Small and rare feldspar grains show undulatory extinction, planar deformation features, and are partly isotropic. Troilite (4 vol. %) and FeNi metal (1.3 vol. %) occur as irregularly shaped grains. Accessory minerals are chromite, ilmenite, and Cl-apatite. A significant portion (1/3) of the stones consist of a dark, fine-grained impact melt containing mineral and chondrule fragments. There are black-colored thin shock veins in both light and dark lithologies. Mineral chemistry: Olivine $\text{Fa}_{27.9 \pm 0.35}$, $N=22$; orthopyroxene $\text{Fs}_{22.8 \pm 0.8}\text{Wo}_{1.30 \pm 0.26}$, $N=17$; feldspar Ab_{86} ; chromite $\text{Fe/Fe+Mg}=0.90$, $\text{Cr/Cr+Al}=0.85$ (at %). Major element composition of the light lithology (XRF, ICP-AS, wt. %): Si=18.3, Ti=0.053, Al=1.12, Cr=0.40, Fe=19.8, Mn=0.26, Ca=1.43, Na=0.74, K=0.11, P=0.10, Ni=1.06, Co=0.046, S=1.7. Atomic ratios of $\text{Zn/Mn} \times 100=1.3$, $\text{Al/Mn}=8.8$. The impact melt lithology has almost the same composition but it is distinctly higher in Ni, Zn, Cu, Mo, Cd, W, Re, Pb, Bi.

MS-XIII) Mount Egerton: It was found at the Norwest of Australia in 1941, and is classified as an aubrite. Aubrites are enstatite achondrites. Most are breccias containing igneous and impact-melted clasts. Like enstatite chondrites, aubrites have highly reduced mineralogy, but they probably do not come from the same parent asteroid as either EH or EL chondrites. It has an abundance of CaS or oldhamite. The metal in Mount Egerton exhibits a very fine pseudo-octahedrite pattern upon etching due to the presence of the Fe-Ni-P-silicide perryite. Perryite only occurs in highly reduced meteorites in which pure magnesian silicates are incorporated in a low-Ni metal host. In contrast to the metal in the main-group aubrites, the metal in Mount Egerton exhibits a mostly chondritic highly siderophile element (HSE) pattern similar to that of enstatite chondrites, particularly that of EL chondrite metal.